Removing Autocorrelation Sidelobes by Overlaying Orthogonal Coding on any Train of Identical Pulses

ELI MOZESON
NADAV LEVANON, Fellow, IEEE
Tel Aviv University

A coherent train of identical linear FM (LFM) pulses is used extensively in radar because of its good range and Doppler resolution. Its relatively high autocorrelation function (ACF) sidelobes are sometimes reduced through spectrum shaping (e.g., nonlinear FM, or intrapulse weighting on receive). We show how to completely remove most of the ACF sidelobes about the mainlobe peak, without any increase to the mainlobe width, by diversifying the pulses through overlaying them with orthonormal coding. A helpful byproduct of this design is reduced ACF recurrent lobes. The overlaid signal also results in reduced Doppler tolerance, which can be considered as a drawback for some applications. The method is applied to several trains of identical pulses (LFM and others) using several orthonormal codes. The effect on the three important properties of the radar signal: ACF, ambiguity function (AF), and frequency spectrum is presented. The effect on Doppler tolerance is studied, and implementation issues are discussed. The new design is also compared with complementary and subcomplementary pulse trains and is shown to be superior in many aspects.

Manuscript received March 22, 2002, revised August 6 and November 4, 2002; released for publication November 4, 2002.

IEEE Log No. T-AES/39/2/813100.

Refereeing of this contribution was handled by P. Lombardo.

Authors' address: Dept. of Electrical Engineering–Systems, Tel Aviv University, P.O. Box 39040, Tel Aviv 69978, Israel.

I. INTRODUCTION

Properties of the ambiguity function (AF) impose fundamental limitations on the ability of any radar waveform of constrained time-bandwidth product to distinguish between two or more targets closely spaced in both range and Doppler or detect targets in the presence of clutter. Designers of radar signals often use trains of compressed pulses to increase effective time bandwidth product and get longer range, better range resolution, or better Doppler resolution.

Coded waveform sets (also known as complementary sets, Welti codes or δ-codes) for enhanced discrimination in range have been studied extensively [1–4]. The important property of complementary sets is that their autocorrelation exhibits zero sidelobes for $t_c \le |\tau| \le T$ and low recurrent lobes (T is the pulse duration and t_c is the coded signal chip length). Sivaswamy [5] introduced a concept of digital and analog basic subcomplementary sequences for pulse compression. The subcomplementary signals exhibit a zero-correlation zone for $\tau \ge \tau_0$ and low recurrent lobes (τ_0 being the duration of the subcomplementary signal kernel). Extending any analog or digital signal with duration τ_0 using simple transformations generates subcomplementary signals. The transformations used are those given by Tseng and Liu [1] to transform a short complementary set into a longer complementary set and are isomorphic to the construction methods of Welti codes [3]. Kretschmer and Gerlach [6] give the same result by stating that for any coded sequence S_0, a subcomplementary set of sequences results from the Kronecker product of S_0 and a matrix consisting of a set of complementary sequences. That result, although stated by Kretschmer and Gerlach for a coded sequence, applies also for analog signals.

We present a new design that, like subcomplementary signals, also results in signals with a zero correlation zone for $t_s \le |\tau| \le T$ and low recurrent lobes. Unlike the previous methods the new approach is based on overlaying an orthogonal coding over any analog or digital signal. The design begins with a train of P identical pulses. The basic original pulse of length T is divided into M slices with a width of $t_s = T/M$. Diversity is then introduced by overlaying orthonormal coding on the M slices in the P pulses. It is shown that the autocorrelation function (ACF) $R(\tau)$ exhibits a zero-sidelobe gap for $t_s \le |\tau| \le T$, independent of the basic pulse waveform. The behavior of the ACF sidelobes remaining over $0 \le |\tau| \le t_s$, the AF, and the reduction in ACF recurrent lobes, are determined by the specific waveform of the basic pulse and by the type of orthonormal coding used.

Sections II and III give definitions of the signal structure and the orthogonal coding and describe

the overlaying method. Sections IV–VII present examples of a train of 8 frequency or phase modulated signals on which we overlay 8-element orthogonal coding (two different orthogonal codes are used in all examples). In Section VIII we compare the new design with Sivaswamy's subcomplementary signals. In Section IX we describe the effect of weighting and in Section X Doppler tolerance is discussed.

II. SIGNAL DEFINITION

We start with a train of P identical coded or analog pulses with pulse length T. Assume the complex envelope of the original pulse $s(t)$ $(0 \le t \le T)$ is divided into M slices with length t_s each $(Mt_s = T)$. Note that this slicing is done with no connection to the original stepped or coded nature of the pulse. Each slice is additionally coded by the elements of an orthogonal P-by-M coding matrix $\mathbf{A}$ where the P rows contain the coding sequence used for the P pulses in the train. The new overlaid signal complex envelope is given by

$$g(t) = \sum_{p=1}^{P}\sum_{m=1}^{M} a_{p,m}s_m[t-(p-1)T_r] \qquad (1)$$

where $a_{p,m}$ is the element of $\mathbf{A}$ used to code the mth slice in the pth pulse in the train $(1 \le m \le M$, $1 \le p \le P)$, T_r is the pulse repetition interval (PRI), and $s_m(t)$ is the complex envelope of the mth slice of the original pulse during $(m-1)t_s \le t < mt_s$ and zero elsewhere.

The coding matrix $\mathbf{A}$ is said to be orthogonal when the dot product between any two columns of $\mathbf{A}$ is zero ($\mathbf{A}^T\mathbf{A}$ is diagonal). An important case is where all elements in the matrix have the same absolute value (normalized to unity) and differ only in their phase denoted by $\varphi_{p,m}$ (in this case we refer to the matrix $\mathbf{A}$ as an orthonormal phase coding matrix). For an orthonormal phase coding matrix $\mathbf{A} = \{a_{p,m}\} = \{\exp(j\varphi_{p,m})\}$ the signal maintains its envelope power properties and we can write that $\mathbf{A}^T\mathbf{A} = P\mathbf{I}$ where $\mathbf{I}$ is an M-by-M identity matrix. Note that the structure of an orthonormal phase coding matrix $\mathbf{A}$ is a sufficient condition for the rows to be a complementary set [6]. However, the opposite is not true-when the rows of $\mathbf{A}$ constitute a complementary set it does not necessarily imply that the columns are mutually orthogonal (e.g. the binary pair $\{1\ 1\ -1\ 1\}\{1\ -1\ -1\ -1\}$ is complementary and $\{1\ 1\}\{1\ -1\}\{-1\ -1\}\{1\ -1\}$ are not all orthogonal). Note also that orthogonal P-by-M matrices $\mathbf{A}$ exist only for $M \le P$ while complementary sets of P sequences with M bits exist also for $M > P$.

Two types of orthonormal codes are demonstrated in (2). On the left hand side a phase coding matrix of a binary orthonormal phase code constructed using nested operations on a 2-element complementary pair is given. Note that due to the construction method the code exhibits a random-like nature. The second type of orthonormal code is based on the complementary set formed from all cyclic shifts of an ideal sequence [7]. An example of an orthonormal code utilizing all 8 cyclic shifts of an 8 element P4 code [6] is given on the right-hand side of (2). Note that the second code is a polyphase code and that it has an ordered nature since the P4 itself is of ordered nature and the use of ordered cyclic shifts adds additional order to the code.

$$\varphi_{\text{binary}} = \pi \begin{bmatrix} 0&0&0&0&0&0&0&0\\ 0&0&1&1&1&1&0&0\\ 0&1&1&0&0&1&1&0\\ 0&0&0&0&1&1&1&1\\ 0&1&0&1&0&1&0&1\\ 0&0&1&1&0&0&1&1\\ 0&1&0&1&1&0&1&0\\ 0&1&1&0&1&0&0&1 \end{bmatrix} \qquad (2)$$

$$\varphi_{\text{P4}} = \frac{\pi}{8} \begin{bmatrix} -1&-4&7&0&7&-4&-1&0\\ -4&7&0&7&-4&-1&0&-1\\ 7&0&7&-4&-1&0&-1&-4\\ 0&7&-4&-1&0&-1&-4&7\\ 7&-4&-1&0&-1&-4&7&0\\ -4&-1&0&-1&-4&7&0&7\\ -1&0&-1&-4&7&0&7&-4\\ 0&-1&-4&7&0&7&-4&-1 \end{bmatrix}.$$

The two explicit examples in (2) are used extensively throughout the work presented here demonstrating some properties of the new design.

III. THE AUTOCORRELATION FUNCTION

The unnormalized, a-periodic ACF $R(\tau)$ of the pulse train is defined as

$$R(\tau) = \int_0^{PT_r} g(t)g^*(t-\tau)dt, \qquad -\infty < \tau < \infty. \quad (3)$$

In the Appendix we show that for $g(t)$ defined by (1) and when $\mathbf{A}$ is an orthonormal phase coding matrix, the partial ACF in the area of the mainlobe (around zero delay) is given by

$$R(\tau) = \begin{cases} P\sum_{m=1}^{M} R_m(\tau) & 0 \le |\tau| < t_s \\ 0 & t_s \le |\tau| < T_r - T \end{cases} \qquad (4)$$

where $R_m(\tau)$ is the autocorrelation of $s_m(t)$. Note that the ACF in the area of the mainlobe is not a function of the order of the slices in the original signal or the orthonormal phase coding matrix used. Different signal variants with the same ACF for $0 \le |\tau| \le T_r - T$

are possible by: 1) permutation of the slices within the pulse, and 2) using a different orthonormal phase coding matrix. The different variants can be used as a means for introducing additional diversity (from batch to batch or between adjacent radars), to lower recurrent lobes, or to get better Doppler behavior. Note also that using different repetition intervals T_r (staggering) does not change the partial autocorrelation in the area of the mainlobe but it can be used to further reduce recurrent lobe peaks with a price of increasing the number of peaks.

Equation (4) states that overlaying orthogonal coding on a train of identical pulses (any kind) removes the autocorrelation sidelobes around the mainlobe, for most of the pulse duration. More accurately, over $(M-1)/M$ of the pulse duration, e.g., $M = 8$ implies that 87.5% of the pulse duration is sidelobe-free. The remaining 12.5% is adjacent to the mainlobe peak. The sidelobe behavior in this remaining delay span depends on the basic pulse waveform. The next sections search for waveforms that lower even those remaining sidelobes.

In many radar applications target Doppler is unknown or multiple returns with different Doppler values are expected. The ACF of the radar signal gives the matched filter normalized response to a zero Doppler target. The AF of a radar signal is a two-dimensional function of delay (τ, seconds) and Doppler (ν, Hz). A cut of the AF for any Doppler gives the normalized response of the matched filter to a non-zero Doppler target. Maybe the most important property of the ambiguity function is that the volume under the ambiguity surface is fixed, i.e., lowering sidelobes anywhere over the delay-Doppler plane will give rise to higher sidelobes at different delay-Doppler locations.

In the next sections we give examples of the AF, autocorrelation and spectrum for several signals designed with the new method. We first consider signals that have a continuous phase during each slice. The most simple signal is one for which the signal phase is constant during the slice. For this case (denoted Case 0) the ACF for any slice is not a function of the constant phase used for that slice and is given by a triangle function. Case 0 is of no interest and is not discussed. In Case I the basic signal is a stepwise linear FM (LFM) pulse, constructed from 40 steps (5 steps in each one of the 8 slices). It effectively covers also the case when the number of steps in a slice is infinity or just one step. The nonlinear phase change is further generalized in Case II and Case III where we give examples of an LFM-LFM, continuous NLFM signals and NLFM-LFM signal. The definitions of LFM-LFM and NLFM-LFM signals are given in the corresponding sections.

Second we consider phase-coded signals where the phase may switch its value during the slice. We give an example of a Barker and a nested Barker signal (Case IV) and an example of a complementary set (Case V).

In the examples given in the next sections we use the two 8×8 overlay codes explicitly given in (2). For simplicity of writing we denote the first code as the binary code and the second code as the P4 based code. Some results with quaternary codes, codes with $M = P > 8$, $M < P$, generalized P4, P3, Frank [6] and Golomb [8] based complementary sets are also mentioned.

IV. CASE I. LINEAR FREQUENCY MODULATED PULSE

Consider the case where the basic signal is a stepwise LFM pulse with 40 steps and the total bandwidth is set such that the first null in the autocorrelation plot is at $T/40 = t_s/5 = t_b$. Fig. 1 shows the frequency (top) of the basic pulse, and phase history of all pulses overlaid with the binary-based orthogonal code given in (2) (solid). The dotted phase plot resulted from the orthogonal code based on all 8 consecutive cyclic shifts of an 8-element P4. The two corresponding partial AFs for $-Mt_s \le \tau \le Mt_s$ and $0 \le \nu \le 1/T_r$ are given in Fig. 2 using a logarithmic scale. The full autocorrelation and autocorrelation zoom for the first slice are shown in Fig. 3. The repetition interval (T_r) used for the plots was $3T$ (33% Duty cycle).

Note that the signal can be looked at as an identical slice signal with linear frequency hopping between slices. In the Appendix (corollary 3) we show that in this case the partial ACF can be written as

$$R(\tau) = \rho(\tau)\frac{\sin(\pi M \Delta f \tau)}{\sin(\pi \Delta f \tau)} \tag{5}$$

where $\rho(\tau)/M$ is the ACF of a single 5-step LFM slice and Δf is the frequency shift between slices ($\Delta f T = 5$ gives a first null at $t_s/5$). Note that since the frequency change within the slice times the slice duration is only 0.5 the slice ACF $\rho(\tau)/M$ is very close to that of a constant frequency slice (a triangle) and the autocorrelation mainlobe width and sidelobes are mostly characterized by the $\sin(\pi M \Delta f \tau)/\sin(\pi \Delta f \tau)$ term in (5). This explains why, though not shown, the autocorrelation and spectrum do not change much when continuous LFM is used instead of 5 steps/slice or when a single frequency value is used for each slice (frequency hopping from slice to slice). The subject of further reducing the sidelobe level by shaping $\rho(\tau)$ (and increasing the time bandwidth product within the slice) is addressed in the next section.

Notice that the first autocorrelation sidelobe level is -15.9 dB while for a train of identical LFM pulses, without orthonormal coding, the sidelobe

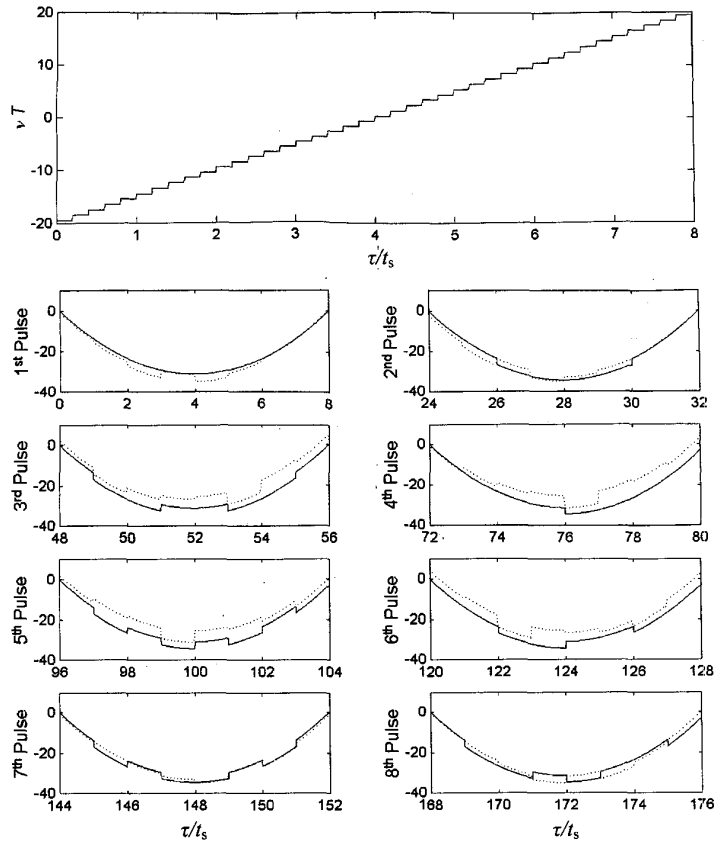

Fig. 1. Original pulse frequency history (top) and all pulse phase history for stepwise linear frequency pulse train overlaid with 8×8 binary (solid) or P4 based (dotted) orthonormal phase code. 40 frequency steps. Bandwidth designed to give first autocorrelation null at $t_s/5$.

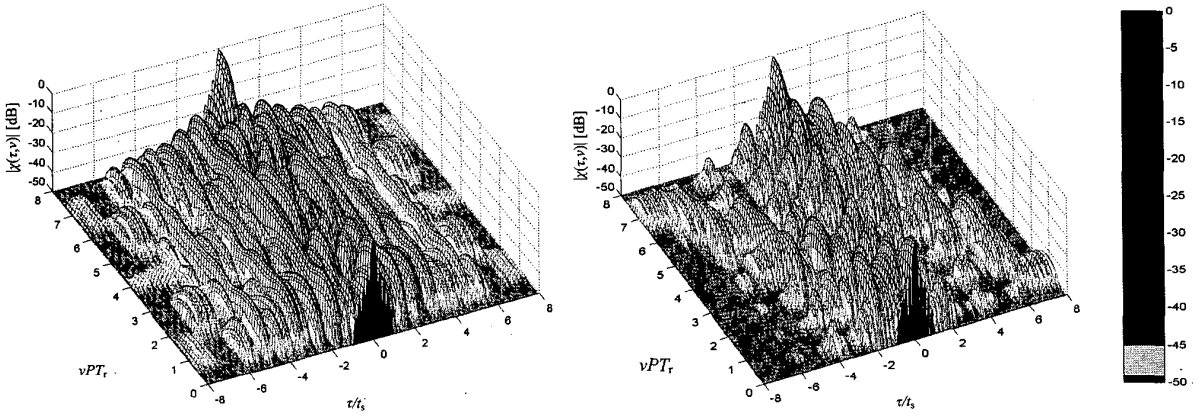

Fig. 2. Partial AF of linear stepwise frequency pulse train overlaid with 8×8 binary (left) or P4 based (right) orthonormal phase code.

level is -13.6 dB. Note also that the autocorrelation recurrent lobe level shown on the lower part of Fig. 3 (P4 based coding) is misleading since the AF cut at non-zero Doppler could show a much higher recurrent lobe peak (close to 0 dB) due to the cyclic shift structure of the overlaid code and the original pulse frequency history. These AF sidelobes can be reduced by permutations of the slices and changes to the slice slope direction of the basic LFM pulse. Such a modification will not change the ACF in the area of the mainlobe. Note that reducing these AF sidelobes is not always necessary since the Doppler value where they occur can be made much higher than the expected Doppler returns.

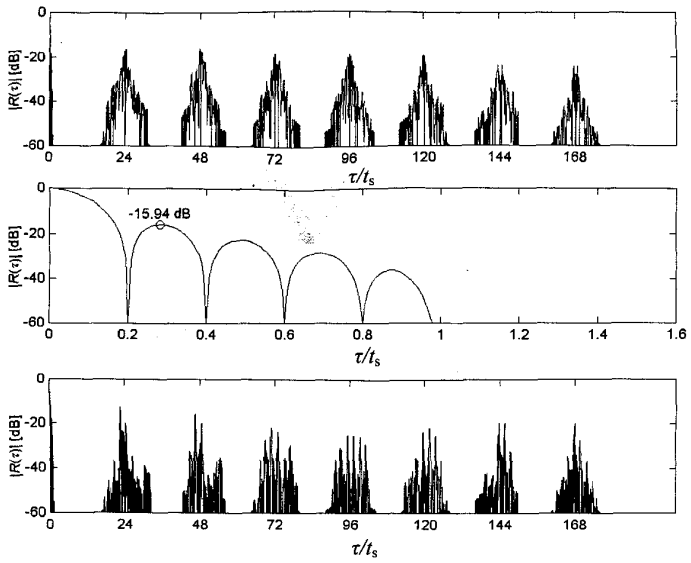

Fig. 3. Autocorrelation mainlobe zoom (center) and full autocorrelation of linear stepwise frequency pulse train overlaid with 8×8 binary (top) or P4 based (bottom) orthonormal phase code.

The partial AF plot of a LFM pulse train with and without orthogonal coding is shown in Fig. 4. The figure shows the partial ambiguity plot of the signal with the two types of overlaid orthogonal coding (center and bottom part) and without coding (top) for $0 \leq \nu \leq 1/T_r$ (left) and $0 \leq \nu \leq 1/PT_r$ (right).

Note in Fig. 4 how orthonormal phase coding shifts volume of the AF from the zero-Doppler axis to higher Doppler (the overall volume under the ambiguity surface squared remains fixed). For the binary coding the volume is distributed almost evenly over all non-zero Doppler values (Fig. 4, center) while for the ordered P4 based coding the volume is moved to a diagonal ridge (Fig. 4, bottom). Note also the secondary peaks close to zero delay in the lower left partial ambiguity plot. These peaks are a by-product of the P4 code and the diagonal ridge that results from it. Note also that, though not shown, cyclically permuting the pulses in the pulse train or changing the direction of the P4 code (flipping the original P4 code head-to-tail) has an effect on portions of the partial AF shape, the signal spectrum and autocorrelation recurrent lobes but does not change its general behavior in all those aspects. Note, though not shown, that using opposite direction cyclic shifts or the conjugate P4 code results in rotating the AF diagonal ridge in 90° (extending from the center peak to the first and third quadrants instead of the second and fourth quadrant). Note also that using generalized P4 [6] code where the relatively prime integer to M is not $\pm 1 \pmod{M}$ results in splitting the ridge to several smaller parallel ridges such that the partial ambiguity plot has a shape closer to that of the binary coded LFM pulse train.

Finally note that increasing M and P results in sharper ridges and lower sidelobes between the ridges. This is exemplified in Fig. 5 showing the partial AF of a P4 based orthogonal coded pulse train where the number of pulses and slices was doubled ($M = P = 16$).

We can compare the proposed signal with two coded pulse trains that give the same mainlobe width (same bandwidth) and similar ridged partial AF. Signal 1 is a pulse train utilizing all (40) cyclic shifts of a 40 element P4. Signal 2 is constructed from 8 consecutive cyclic shifts of a 40 element P4. The two coded waveforms though having the same mainlobe width and similar ridged partial AF as the proposed design, suffer from significant drawbacks in the form of using 40 pulses in the train instead of 8 (signal 1), or less effective spectrum shape, higher autocorrelation recurrent lobes peaks, and high autocorrelation sidelobes (signal 2).

Note also that the ridge shape of the partial AF for a P4 based code is a function of using both P4 and consecutive cyclic shifts. When the pulses in the pulse train are permutated (all cyclic shifts are used but not in a consecutive order) or when all consecutive cyclic shifts of other random natured ideal sequence are used instead of the ordered P4 (e.g. Golomb with $M = P = 7$) the partial AF does not have the diagonal ridge and the volume is spread over all non-zero Doppler values.

Using other ordered codes (instead of P4) such as P1 (Frank) or P3 [6] resulted in similar partial AF plot (position of AF peaks along the diagonal ridge and peaks value is slightly different).

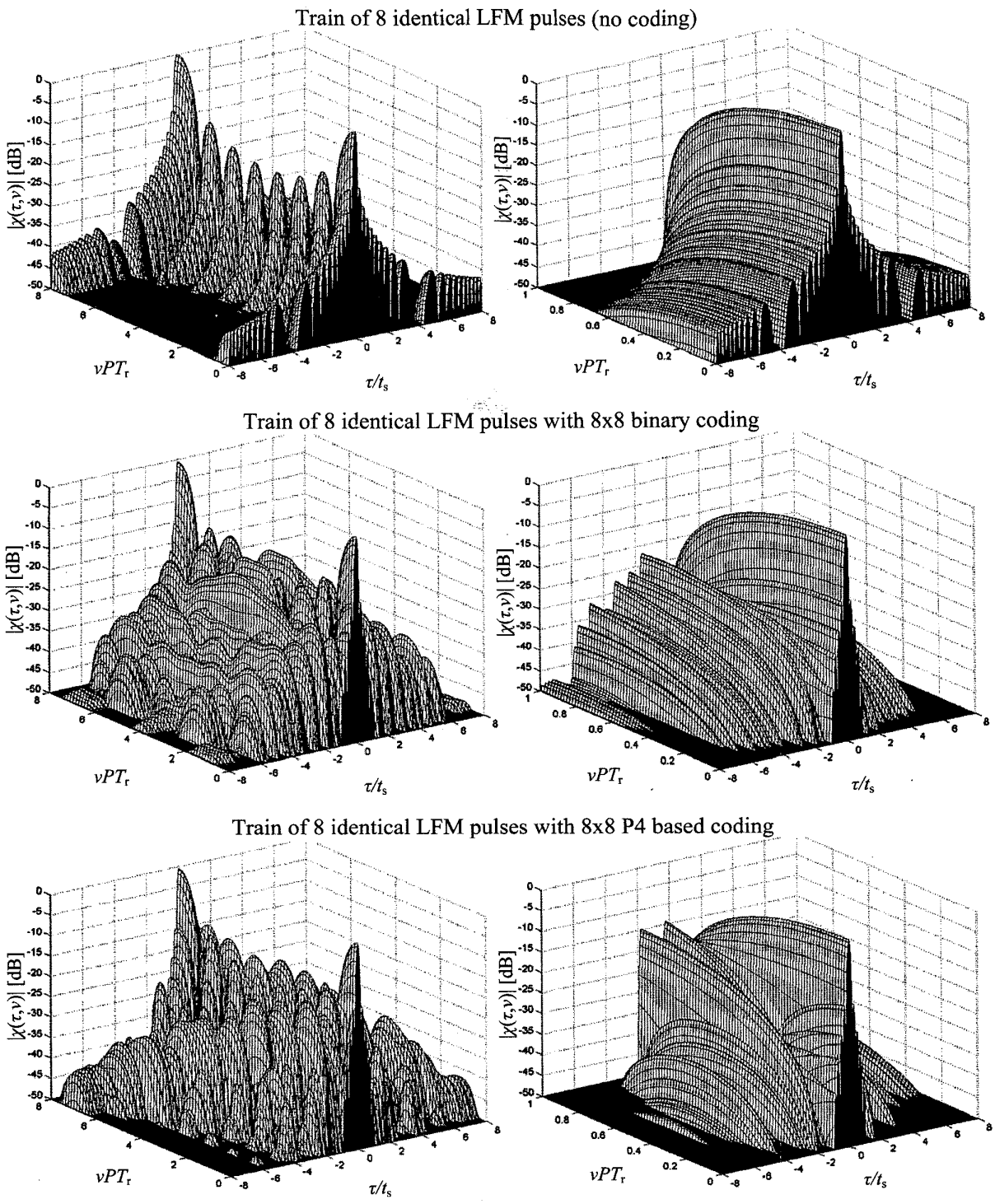

Fig. 4. Partial ambiguity plot of LFM pulse train without orthogonal coding (top) and with two types of orthogonal coding (binary-center, P4 based-bottom) for $0 \le \nu \le 1/T_r$ (left) and $0 \le \nu \le 1/PT_r$ (right).

V. CASES II AND III. LFM-LFM AND LFM-NLFM ORTHONORMAL PHASE-CODED TRAINS

Consider an orthonormal phase-coded pulse train where each slice is an LFM pulse and the slices are also linearly frequency shifted (see Fig. 6, top). This signal is named an LFM-LFM orthonormal phase coded pulse train. Denote the slice frequency deviation B and the frequency shift between slices Δf. The total pulse frequency deviation is given

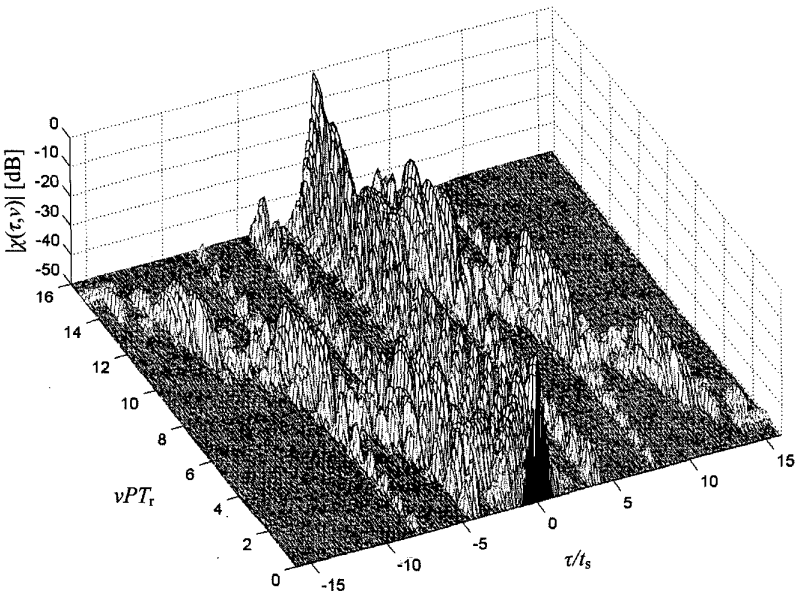

Fig. 5. Partial AF of a P4 based LFM coded pulse trains using $M = P = 16$.

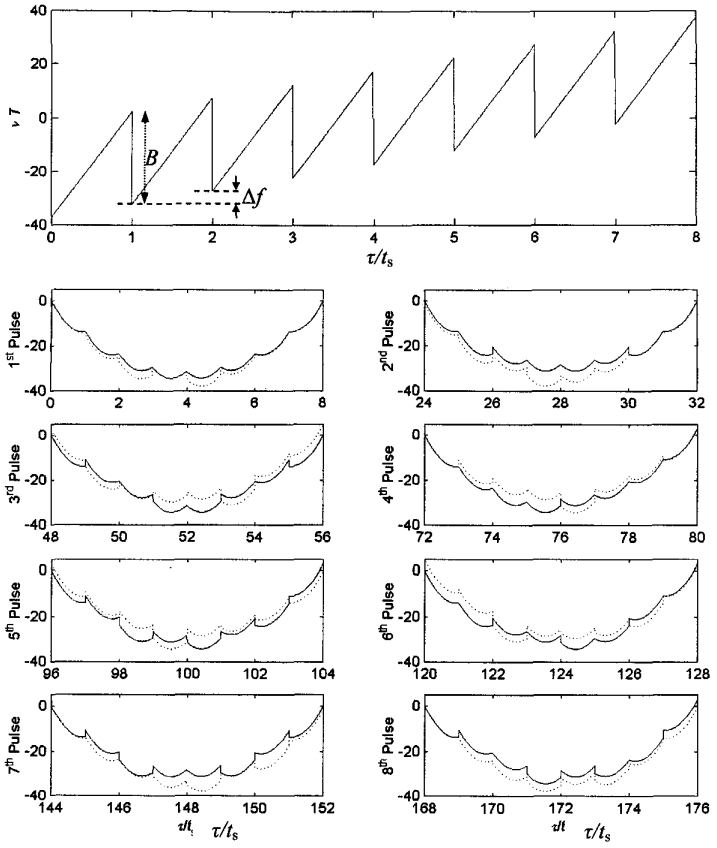

Fig. 6. Original pulse frequency history (top) and all pulse phase history for minimum peak sidelobe LFM-LFM pulse train overlaid with 8×8 binary (solid) or P4 based (dotted) orthonormal phase code.

by $(M-1)\Delta f + B$. Note that in the continuous orthogonal phase-coded LFM signal described in the previous section $\Delta f = B$ and in the continuous LFM Sivaswamy subcomplementary signal [5] all slices are identical and $\Delta f = 0$. Note also that the LFM-LFM construction effectively shapes the signal spectrum because the instantaneous frequency histogram has higher values near the center frequency. Using

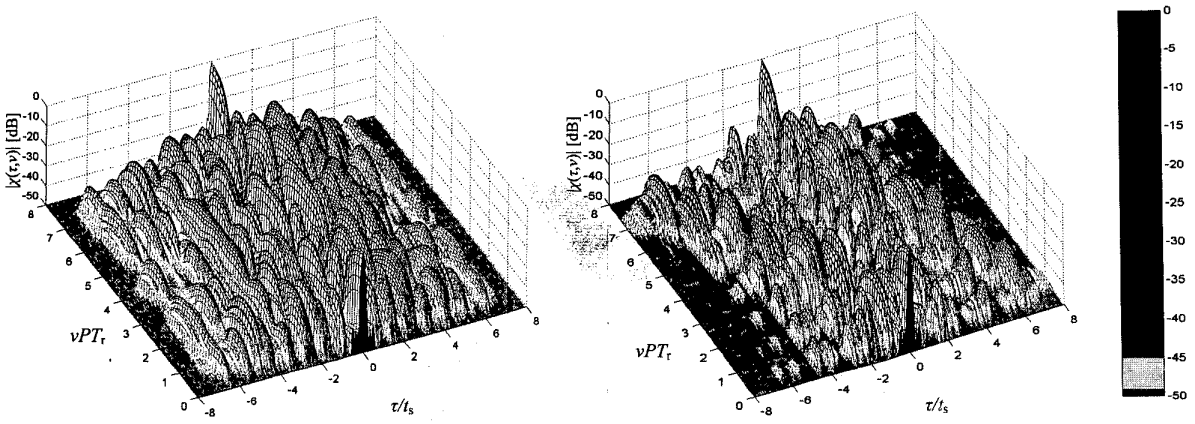

Fig. 7. Partial AF of minimum peak sidelobe LFM-LFM pulse train overlaid with 8×8 binary (left) or P4 based (right) orthonormal phase code.

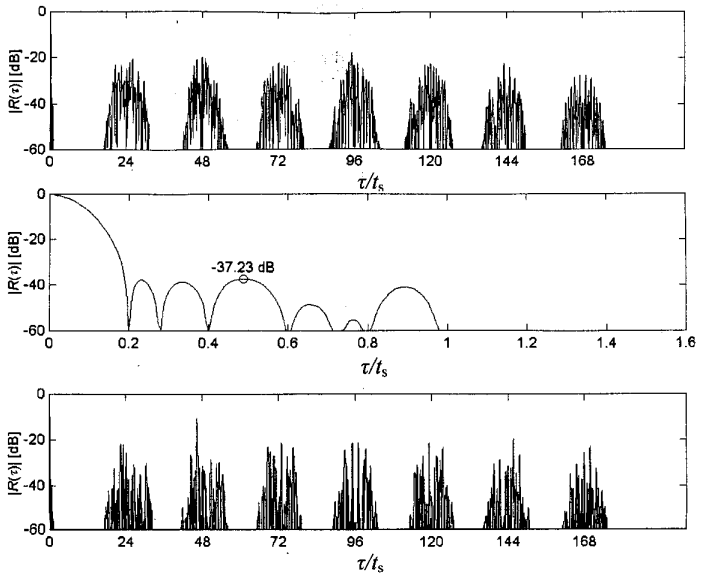

Fig. 8. Autocorrelation mainlobe zoom (center) and full autocorrelation of minimum peak sidelobe LFM-LFM pulse train overlaid with 8×8 binary (top) or P4 based (bottom) orthonormal phase code.

corollary 3 in the appendix it is easy to show that for the LFM-LFM signal the normalized partial ACF for $0 \le \tau \le t_s$ is given by

$$R(\tau) = \frac{1}{M} \frac{\sin(\pi B \tau (1 - \tau/t_s))}{\pi B \tau} \frac{\sin(\pi M \Delta f \tau)}{\sin(\pi \Delta f \tau)}. \quad (6)$$

Using the relatively simple expression for the ACF, we minimize the peak sidelobe for $t_s/5 < \tau < t_s$ while holding the first null fixed at $t_s/5$ as in the previous examples (B and Δf are the free parameters). Minimum peak sidelobe level for $M = 8$ is -37.23 dB (obtained for $B = 4.96/t_s$ and $\Delta f = 5/T$). The total frequency deviation normalized by the pulse duration in this case is 74.68. When using 16 slices per pulse ($P = M = 16$) we limit the mainlobe to $t_s/2.5$ and get minimum peak sidelobe of -41.7 dB (obtained for $B = 4.16/t_s$ and $\Delta f = 5/T$) with total frequency deviation (normalized by the pulse duration) of 104.1. When we keep increasing $M(= P)$ the minimum peak sidelobe is reduced but with an increase in the overall frequency deviation. When $M = P = 40$ the slice width becomes the mainlobe width and the remaining sidelobes vanish (the resulting signal is then a 40×40 complementary pulse train).

Fig. 6 shows the frequency and phase history of the minimum peak sidelobe LFM-LFM pulse with $B = 4.96/t_s$ and $\Delta f = 5/T$ overlaid with the binary orthonormal phase code and the P4 based orthonormal code. The partial AF for $-Mt_s \le \tau \le Mt_s$ and $0 \le \nu \le 1/T_r$ are given in Fig. 7 using a logarithmic scale. The full autocorrelation and autocorrelation zoom for the first slice are shown in Fig. 8. The repetition interval (T_r) used for the plots was $3T$ (33% Duty cycle). Comparing the middle plots in Fig. 3 and Fig. 8 note that the new ACF not only has lower

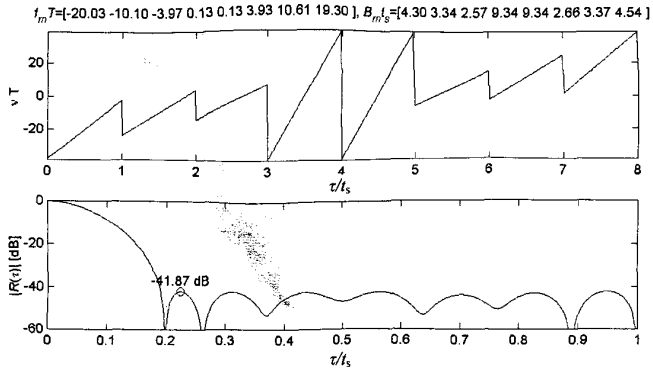

Fig. 9. Global minimum peak sidelobe LFM-NLFM orthonormal phase-coded pulse train frequency history (top) and autocorrelation mainlobe (bottom). Maximal time-frequency span product of 74.58 and first null at $t_s/5$.

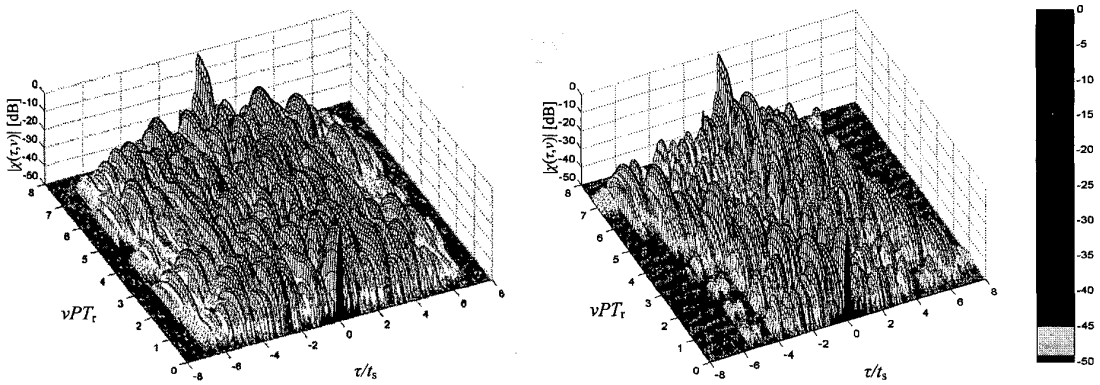

Fig. 10. Partial AF of minimum peak sidelobe LFM-NLFM pulse train overlaid with 8×8 binary (left) or P4 based (right) orthonormal phase code.

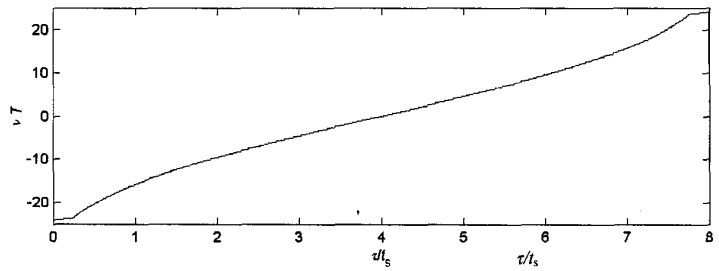

Fig. 11. Original pulse frequency history for NLFM signal designed for minimum peak sidelobe level and first null at $t_s/5$ when overlaid by 8×8 orthogonal code.

peak sidelobes but also has more nulls in the sidelobe pattern. The position of the nulls can be adapted to different positions by changing B or Δf from batch to batch with a small change to the peak sidelobe level.

In the case of the random-natured binary coding, the ambiguity plot (Fig. 7 left-hand side) has a tent shape similar to the shape for LFM orthonormal phase-coded signal (Fig. 2 left-hand side) but has lower values for higher delay (note the low partial ambiguity strip for $|\tau| \geq (M-1)t_s$). When the coding is based on consecutive cyclic shifts of P4 (Fig. 7 right-hand side) we can notice the diagonal ridge and some additional lower ridges parallel to the Doppler axis.

The LFM-LFM construction effectively shapes the signal spectrum because the instantaneous frequency histogram has higher values near the center frequency. This can be further generalized by allowing B, Δf or both to change from slice to slice. We refer to this generalized case (case III) as LFM-NLFM signal (each slice is LFM, but the slopes and bandwidths are changed nonlinearly between slices). It can be shown, using the tools given in the Appendix, that for the LFM-NLFM signal the normalized partial ACF for $0 \leq \tau \leq t_s$ is given by

$$R(\tau) = \sum_{m=1}^{M} \exp(j2\pi f_m \tau) \frac{\sin[\pi B_m \tau(1-\tau/t_s)]}{\pi B_m \tau} \quad (7)$$

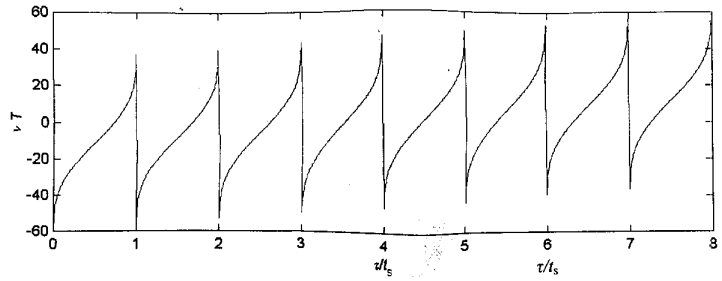

Fig. 12. Original pulse frequency history of NLFM-LFM pulse designed at $t_s/5$ first null and minimum peak sidelobe when overlaid with 8×8 orthonormal phase code.

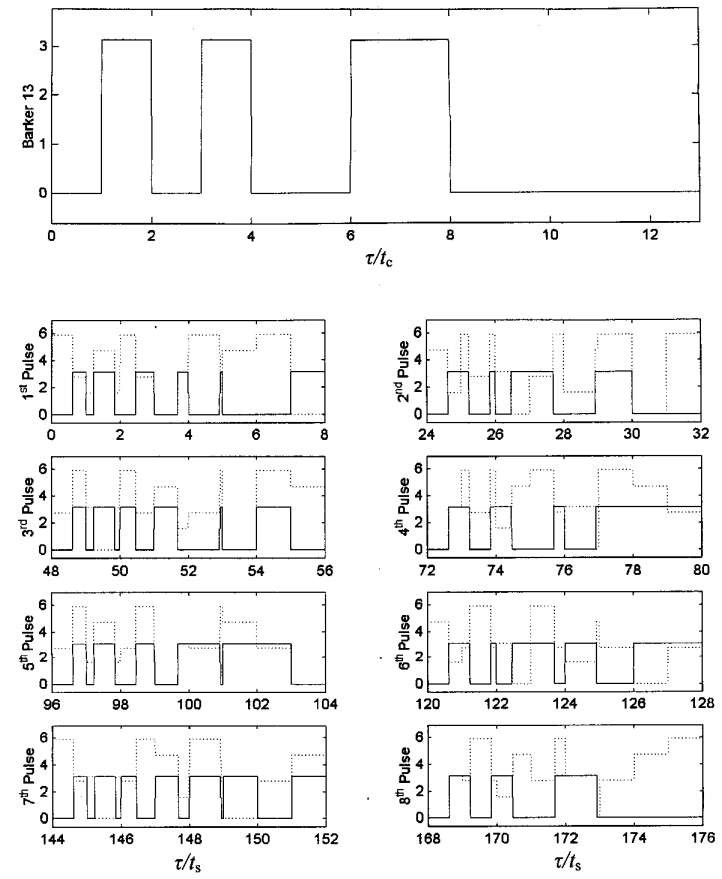

Fig. 13. Phase of original Barker pulse and eight pulses overlaid with 8×8 binary (solid) or P4 based (dashed) orthonormal phase code.

where B_m and f_m are respectively, the frequency deviation and center frequency of the mth slice. Changing the sign of B_m (slope direction), or the order of slices does not change the ACF but affects the signal spectrum and AF. Fig. 9 shows an example of an orthonormal phase-coded LFM-NLFM signal with minimum peak sidelobe for $\tau \geq t_s/5$, where the pulse time bandwidth product is limited to the one of the minimal peak sidelobe LFM-LFM pulse (The global minimum was found using numerical methods).

The optimization lowers the autocorrelation peak sidelobe to -41.87 dB. Allowing the overall signal frequency deviation to take higher values will further decrease the obtainable minimum peak sidelobe level. For maximal time-frequency span product of 80 and 90 we found minimum peak sidelobes of -43.6 dB and -47.33 dB, respectively. Note that we set all slopes to be positive and arranged the slices in the most symmetrical ordered way we found applicable. Changing the order of slices or slope direction will not change the ACF in the mainlobe area (there are $2^M M!$ options for permuting the slices and changing slope directions).

The partial ambiguity shape for both types of overlay code is shown in Fig. 10. Note that for the P4 based code the diagonal ridge is less prominent

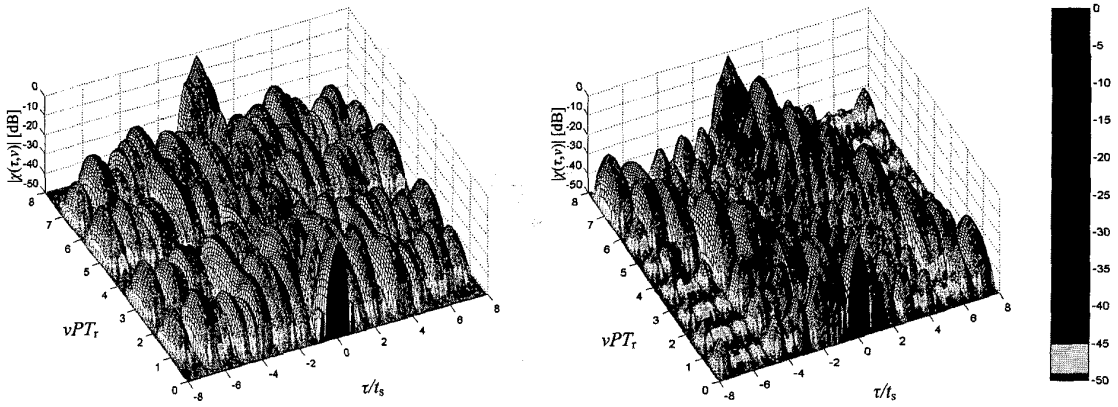

Fig. 14. Partial AF of 13 element Barker pulse train overlaid with 8×8 binary (left) or P4 based (right) orthonormal phase code.

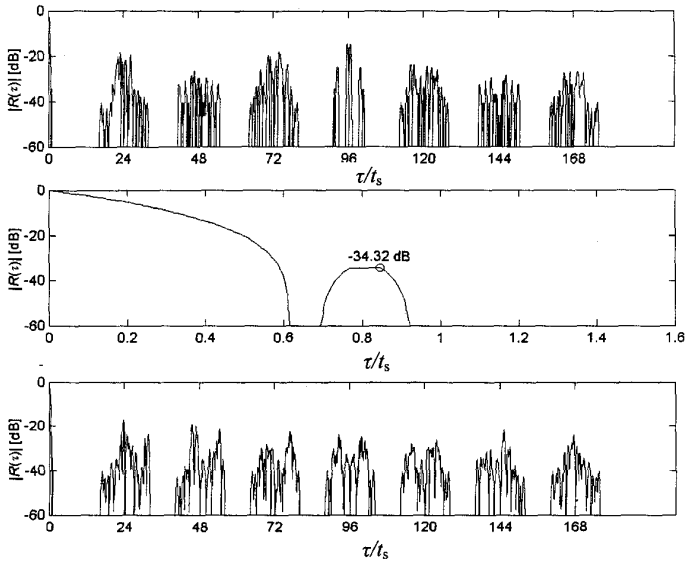

Fig. 15. Autocorrelation mainlobe zoom (center) and full autocorrelation of 13 element Barker pulse train overlaid with 8×8 binary (top) or P4 based (bottom) orthonormal phase code.

especially at lower delay values. We reiterate that the partial AF is affected by the order of slices and slope direction as well as by using different PRI values between the different pulses in the train.

Instead of using LFM, a nonlinear modulation rule is often used such that the spectrum is shaped to a desirable function and the ACF has low range sidelobes. We searched for NLFM and NLFM-LFM designs (see Figs. 11 and 12) which maintained a first null at $t_s/5$ and are optimal in the sense of peak sidelobe. The signal in Fig. 11 yielded peak sidelobe of -24.5 dB. The signal in Fig. 12 yielded peak sidelobe of -36.2 dB.

VI. CASE IV. PHASE CODED PULSE

Consider the case where the original pulse is phase-coded instead of being a continuous frequency modulated or stepped frequency-coded signal. A simple example is a Barker code. First consider a Barker code with length 13 (note that since the pulse is sliced to $M = 8$ slices, the slice and the Barker element length are not the same). The structure of the Barker 13 original pulse before and after orthonormal phase coding using 8 slices is shown in Fig. 13.

The partial AF for $-Mt_s \leq \tau \leq Mt_s$ and $0 \leq \nu \leq 1/T_r$ is given in Fig. 14 using a logarithmic scale. The full autocorrelation and autocorrelation zoom for the first slice $|\tau| \leq t_s$ are shown in Fig. 15. Note that the orthonormal phase-coded Barker 13 has a sidelobe peak of -34.3 dB (compared to -22.2 dB for a train of 8 identical Barker 13 pulses or a single Barker 13 pulse) and the same mainlobe width as a Barker 13 pulse ($T/13 = 8t_s/13$).

A different approach is to use coded sequences with the slice length being an integer multiple of the

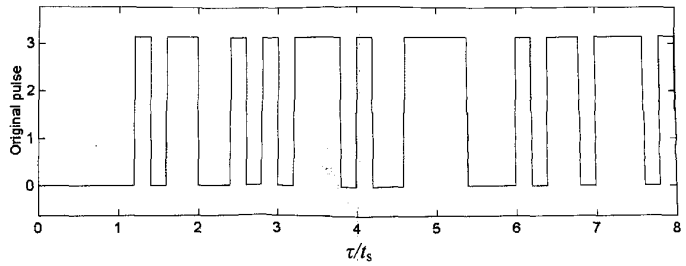

Fig. 16. Phase of basic pulse (40 elements) resulting from complementary set of 8 sequences with 5 elements each.

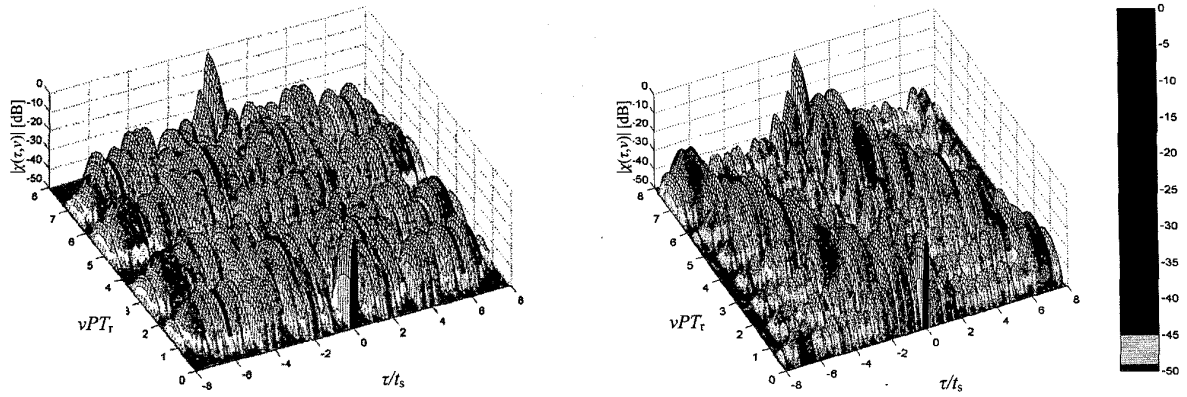

Fig. 17. Partial AF of binary 8×40 complementary set derived from binary 8×5 complementary set overlaid with 8×8 binary (left) or P4 based (right) orthonormal phase code.

bit length. An example of such sequence is a nested Barker sequence of length 5×8 (Barker sequences of length 8 used as the elements of a Barker sequence of length 5).

We did not find a method, other than exhaustive search, for finding phase-coded waveforms that, after being overlaid with an orthonormal phase code, give any desired sidelobe behavior, AF or spectrum.

VII. CASE V. PHASE CODED COMPLEMENTARY SET

When the M slices form a K element (chip) phase-coded complementary set, the proposed design uses the orthogonal phase coding to transform M complementary sequences with K elements to P complementary sequences with MK elements each. The ACF is zero for $t_s/K \le \tau \le t_s$ as well as $t_s \le \tau \le T_r - Mt_s$. Note that complementary sets exist only for specific values of $K \ge M$ [2, 3].

An example of an $M = 8$ sequences $K = 5$ elements complementary set pulse overlaid with our standard orthogonal phase coding is given next. The original pulse has 40 chips taken from the columns of matrix **A** given in (2) when rows 1–3 were erased (thus forming a complementary set of 8 sequences with 5 elements each). The resulting original pulse is thus {+++++ +−+−− ++−+− +−−−+ −++−− −−+++ −+−−+ −−−+−}. The pulse is sliced into 8 slices (5 chips in a slice) and the orthogonal coding is used to modulate 8 pulses.

The signal phase code is shown in Fig. 16. The partial AF for $-Mt_s \le \tau \le Mt_s$ and $0 \le \nu \le 1/T_r$ is given in Fig. 17 using a logarithmic scale. The full autocorrelation and mainlobe area are shown in Fig. 18. Even though the complementary pulse train achieves the largest zero sidelobe gap, the main drawbacks are in the relatively high sidelobes seen in the ambiguity plot for non-zero Doppler and the sinc spectrum shape with first null at $K/t_s = 1/t_c$ (the spectral shape is discussed in the next section).

VIII. COMPARISON WITH SUBCOMPLEMENTARY SIGNALS

In [5] Sivaswamy gives subcomplementary signals with similar structure to the one presented in this paper. Unlike the designs presented here, Sivaswamy's subcomplementary signals are designed such that 1) the slices are identical, and 2) the M element P pulse code is a complementary set. The design presented here requires orthogonality of the code (a demand stronger than the demand for a complementary set) but does not require identity of the slices.

We compare the ambiguity plot of the orthonormal phase-coded stepwise LFM pulse train described in Section IV with the Sivaswamy [5] subcomplementary signal based on stepwise LFM pulse. Fig. 19 gives the

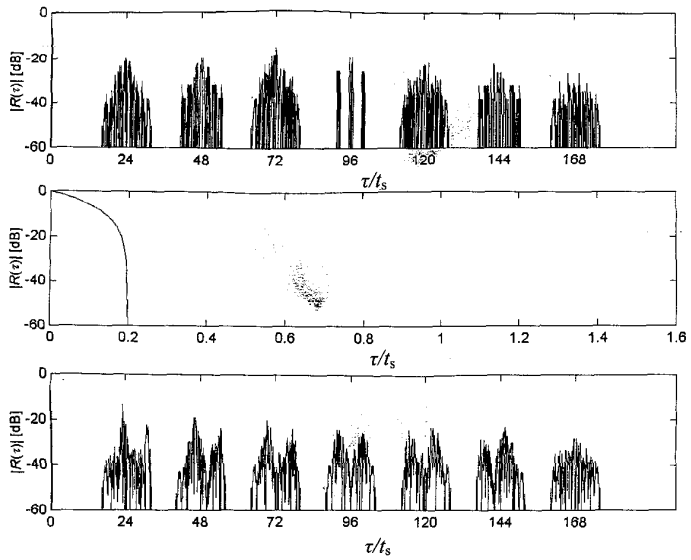

Fig. 18. Autocorrelation mainlobe zoom (center) and full autocorrelation of binary 8×40 complementary set derived from binary 8×5 complementary set overlaid with 8×8 binary (top) or P4 based (bottom) orthonormal phase code.

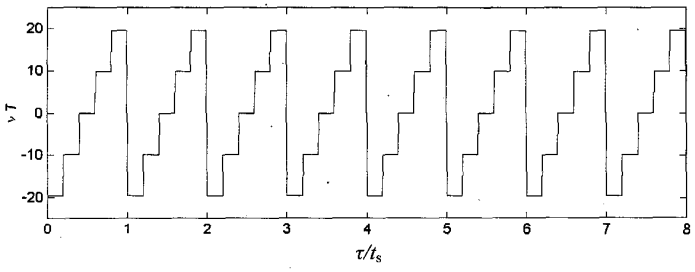

Fig. 19. Original pulse frequency history of stepwise LFM Sivaswamy subcomplementary signal.

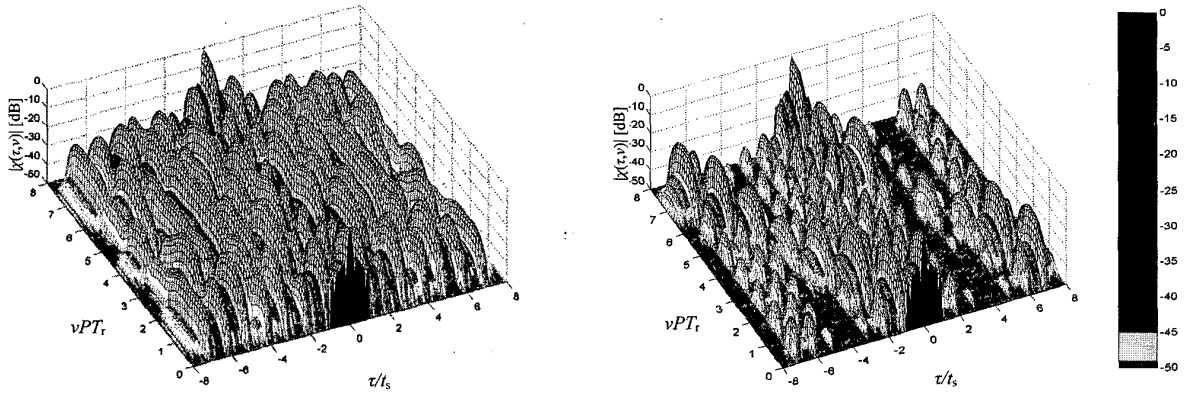

Fig. 20. Partial AF of Sivaswamy subcomplementary signal based on 5 step LFM coded with 8×8 binary (left) or P4 based (right) orthonormal phase code.

frequency history, Fig. 20 the partial AF and Fig. 21 the ACF of Sivaswamy's subcomplementary stepwise LFM pulse train with the same coding used for the new design. The parameters of Sivaswamy's signal were designed to yield the same mainlobe width as our orthonormal phase-coded stepwise LFM pulse train.

Note the higher sidelobes in the partial ambiguity plot (compare Fig. 20 to Fig. 2). The near sidelobe autocorrelation shape has fewer nulls than the partial

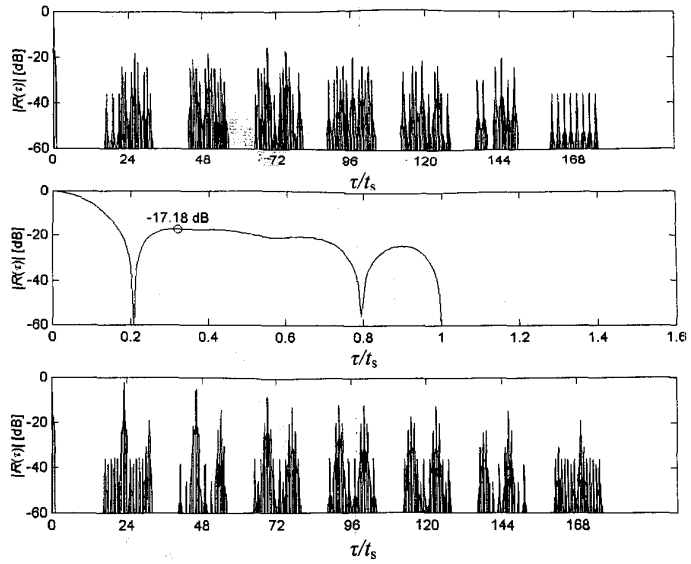

Fig. 21. Autocorrelation mainlobe zoom (center) and full autocorrelation of Sivaswamy subcomplementary signal based on 5 step LFM coded with 8×8 binary (top) or P4 based (bottom) orthonormal phase code.

autocorrelation of the orthonormal phase-coded LFM pulse train and the peak sidelobe is -17.18 dB. The autocorrelation recurrent lobes with ordered P4 based coding have relatively high peaks that are not present in our design.

Comparing the continuous LFM Sivaswamy subcomplementary signal with a continuous LFM orthonormal phase-coded pulse train when the mainlobe width is kept $t_s/5$ gives a first sidelobe level of -16.9 dB (-15.9 dB for the orthonormal phase-coded LFM pulse train), and an ambiguity plot not much different from the one given for the subcomplementary stepwise LFM signal (Fig. 20).

Note also when using binary based orthogonal coding the LFM coded pulse train partial AF has a triangular shape (peaks reduce logarithmically as the delay increases) while the Sivaswamy subcomplementary pulse train signal has a pedestal-shaped partial AF (peaks remain at the same level even when delay increases). In hindsight this should be of no surprise since the coding only distributes the volume under the AF differently for any delay but does not move ambiguity volume from one delay strip to another (the ambiguity volume distribution for different delays remains the same as for the signal prior to coding).

Fig. 22 compares the frequency spectrums of 1) the orthogonal coded LFM pulse train, 2) train the Sivaswamy subcomplementary pulse train, 3) the LFM-LFM orthogonal coded pulse, and 4) the complementary phase-coded pulse train set. All frequency spectrums were calculated by taking the discrete Fourier transform (DFT) of a zero padded version of the signals described in Figs. 1, 6, 16, and 19 using the P4 based orthogonal coding (the signals were all padded to 32 times their length and the signal energy was the same for all signals). Note the orthogonal coded LFM pulse train has the lowest effective bandwidth (though not shown the spectrum of the identical LFM pulse train has slightly lower effective bandwidth). The Sivaswamy subcomplementary pulse train and the LFM-LFM orthogonal coded pulse train have higher effective bandwidth (though not shown, the LFM-NLFM effective bandwidth has slightly higher effective bandwidth than the LFM-LFM orthogonal coded pulse train). The complementary phase-coded pulse train has a sinc-squared spectrum with the largest effective bandwidth and frequency spectrum sidelobe level.

IX. EFFECT OF WEIGHTING

In many radar systems interpulse or intrapulse weighting is often introduced in order to decrease range or Doppler sidelobes with a small increase in mainlobe width and a small decrease in peak response (weighting is usually introduced only at the receiving end). Introducing interpulse weighting to the coded pulse train clearly would destroy the zero sidelobes property for $\tau > t_s$ since the slices would no longer be orthogonal.

The effect of weighting on a 16 pulse 16 slice LFM pulse train overlaid with the P4 based code is demonstrated in Fig. 23. The figure gives the partial ambiguity plot in the area of the mainlobe for no weighting, using only interpulse weighting, using only intrapulse weighting, and using both intrapulse and interpulse weighting. The weighting rule used was a Hamming window (used at the receiving end only). Note how weighting eliminates many of

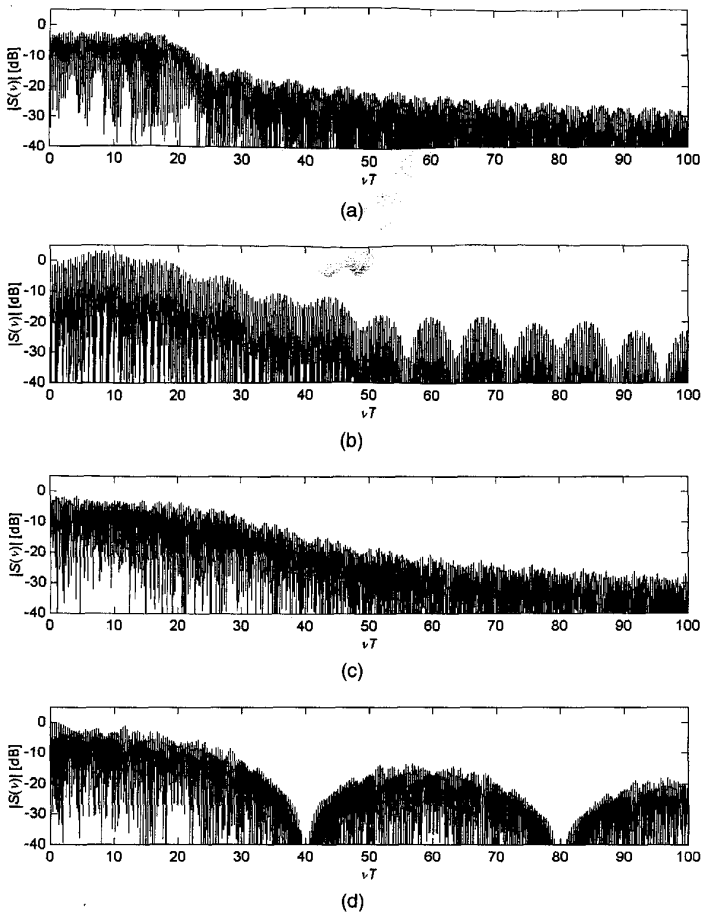

Fig. 22. Frequency spectrum of (a) orthogonal coded LFM pulse train. (b) Sivaswamy subcomplementary pulse train. (c) LFM-LFM orthogonal coded pulse train. (d) Complementary phase-coded pulse train.

the low-level peaks in the partial AF, at a price of widening the stronger peaks along the ridge. Using intrapulse weighting reduces the sidelobe level along the diagonal ridge (between its peaks) and some of the low sidelobes at high delay and low Doppler. The interpulse weighting reduces the low sidelobes forming ridges parallel to the Doppler axis (e.g., at $\tau t_s = 0$, 4 or 8).

Fig. 24 displays the partial correlation showing the change in the near sidelobe level and the loss in the peak response. Note that the interpulse weighting results in the lowest increase to the mainlobe width (first null position increased by 15%), peak sidelobe is 10 dB lower, sidelobes are below 60 dB for delays higher than $2t_s$ and the mismatch loss is 1.54 dB. The intrapulse weighting does not extend the near sidelobe range beyond t_s (the slices are still orthogonal but are no longer orthonormal). It results in a higher mainlobe widening (140% increase to the first null position), the same mismatch loss (1.54 dB) but lower sidelobes (peak sidelobe of only −50 dB). Using both intrapulse and interpulse weighting results in a higher mismatch loss of 3.1 dB, near sidelobes extending below 50 dB for delay above t_s with a peak sidelobe of only −49 dB and a 200% increase in the first null position.

X. DOPPLER TOLERANCE

In many practical situations (e.g. when the radar is used for surveillance) target Doppler is not known and it is required to use several filters (at least P) at the receiver (each matched to a different target Doppler) in order to detect the target return. Generally implementing P filters requires replicating the matched filters construction P times. For Doppler tolerant signals such as a wide bandwidth LFM pulse, a fast Fourier transform (FFT) based filtering method can be used to simplify receiver complexity with almost no loss in the peak response and only a small decrease in the peak-to-sidelobe level ratio. The number of FFT points used should be taken high enough (padding the P signal samples with zeros) to minimize the straddle loss. The principle of FFT processing is schematically described in Fig. 25. Its deviation from ideal Doppler (matched filter)

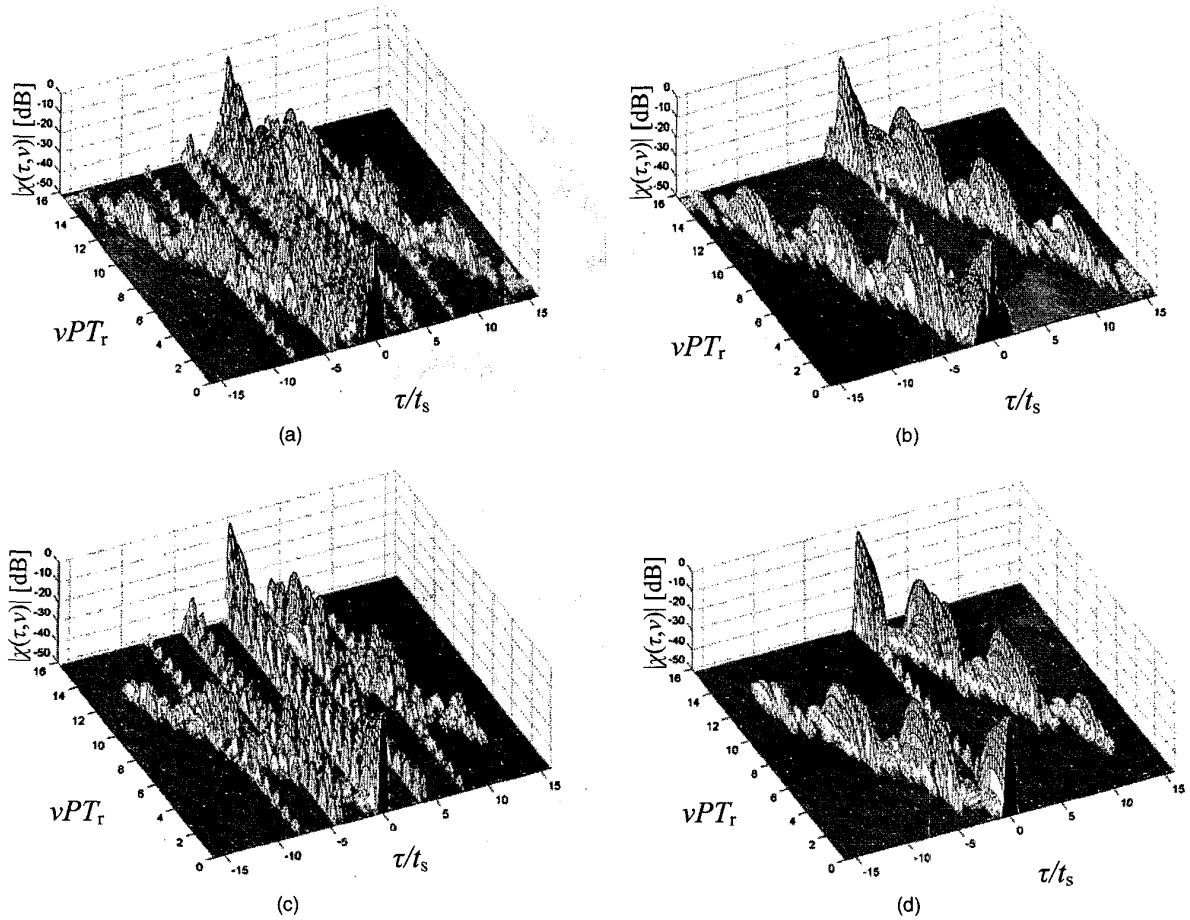

Fig. 23. Effect of weighting on partial AF of 16×16 LFM P4 based orthogonal coded pulse train. (a) No weighting. (b) Interpulse weighting. (c) Intrapulse weighting. (d) Intrapulse and interpulse weighting.

processing results from the simple fact that a matched filter takes into account the phase change within the narrow pulses while the FFT processing is based only on the phase change from pulse to pulse.

Fig. 26 presents simulation results showing the FFT based receiver peak response loss for an identical LFM pulse train (no coding), orthogonal coded LFM pulse train, orthogonal coded LFM-LFM pulse train, and a train of complementary pulses with the same mainlobe width. The receiver peak response loss only due to the waveform is presented (FFT straddle loss is minimized by using 128 FFT points in the simulation and the simulation sampling period is high enough such that the straddle loss due to sampling in time does not affect the results). All signals are 8 pulses, 8 slices/pulse with the P4 based orthogonal code given in (2) and designed to give a first null at $t_s/5$. Using a 16-pulse train with 8 slices or using binary coding instead of a P4 based code gives similar results.

Fig. 26 demonstrates that while the orthogonal coded LFM pulse train exhibits worse loss than noncoded LFM pulse train, its loss is much lower than in the complementary set case.

XI. CONCLUSIONS

A method of diversifying any train of P identical pulses was given. The original pulse was divided into M slices with width t_s, and diversity was obtained by overlaying orthonormal coding on the M slices in the P pulses. Orthonormal overlay removes the autocorrelation sidelobes over $(M-1)/M$ of the pulse duration. We have given some examples of an FM pulse train overlaid with an orthonormal phase code and compared the AF, autocorrelation, and spectrum, to that of a Sivaswamy subcomplementary pulse train, an LFM pulse train with no additional coding and a train of complementary phase-coded pulses. In our examples we used two types of overlay coding—a binary noise-like coding and an ordered coding based on all cyclic shifts of P4. The use of the code based on cyclic shifts of P4 resulted in lower AF sidelobes in the area of the peak response and higher recurrent lobe peaks off zero Doppler.

Three additional signal designs named LFM-LFM, LFM-NLFM, and NLFM-LFM orthonormal phase-coded pulse train were introduced. Analytic

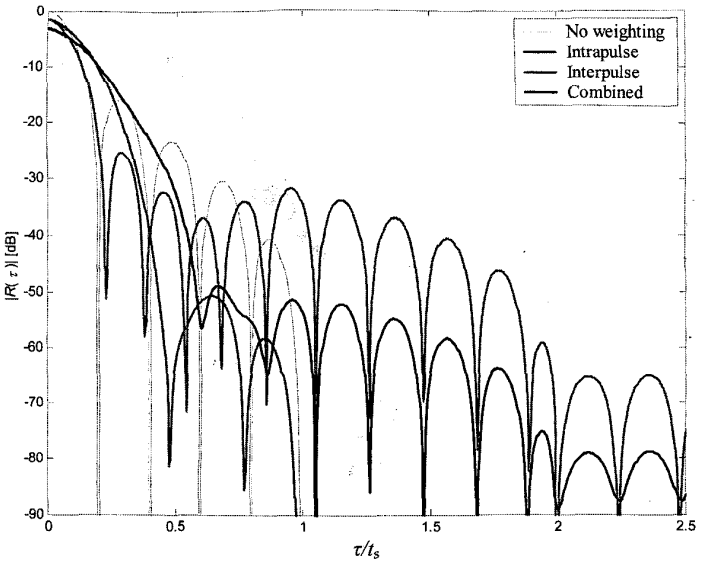

Fig. 24. Effect of weighting on partial correlation of 16×16 LFM P4 based orthogonal coded pulse train.

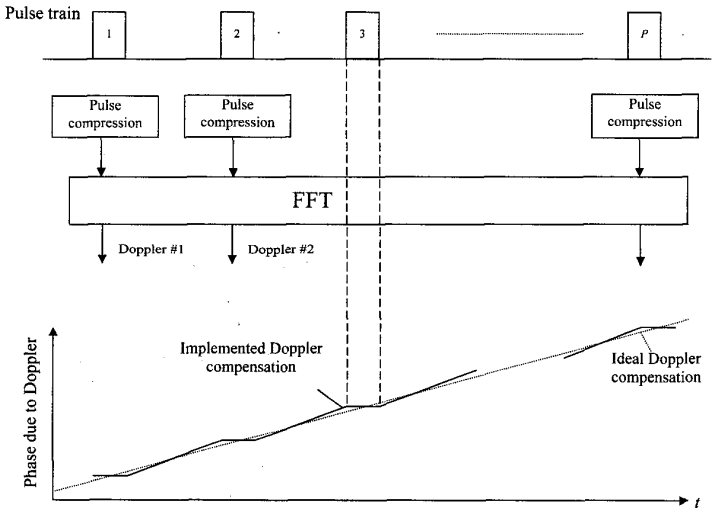

Fig. 25. Schematic description of Doppler processing a radar pulse train using FFT.

expressions for the near sidelobes of the ACF were developed, which help in choosing signal parameters. Examples of overlaying orthonormal phase coding on phase-coded signals were also given. Finding optimal signals of this kind requires an exhaustive search. The new designs were shown to have zero range sidelobes for most of the delay range and low range sidelobes for the remaining delays.

A significant practical advantage of the new FM based waveforms over complementary sets or other phase-coded signals with thumbtack AF is in their improved Doppler tolerance which enables the use of FFT to simplify receiver complexity.

The zero sidelobe location in the AF of the orthonormal phase coded LFM pulse train (zero range-sidelobes at zero Doppler) turns out to complement the AF low sidelobes of a train of identical LFM pulses (low range-sidelobes at non zero Doppler). This suggests using a signal based on both types of waveforms, and instead of using a receiver matched to the whole signal, perform match filtering for each part of the signal separately and then nonlinearly process the matched filters outputs.

APPENDIX. AUTOCORRELATION FUNCTION OF ORTHOGONAL CODED PULSE TRAINS

Here we give explicit formulation of the ACF for any delay and some specific results for areas that are of more interest.

The ACF is calculated using (1) in (3). Rearranging the order of summation and integration,

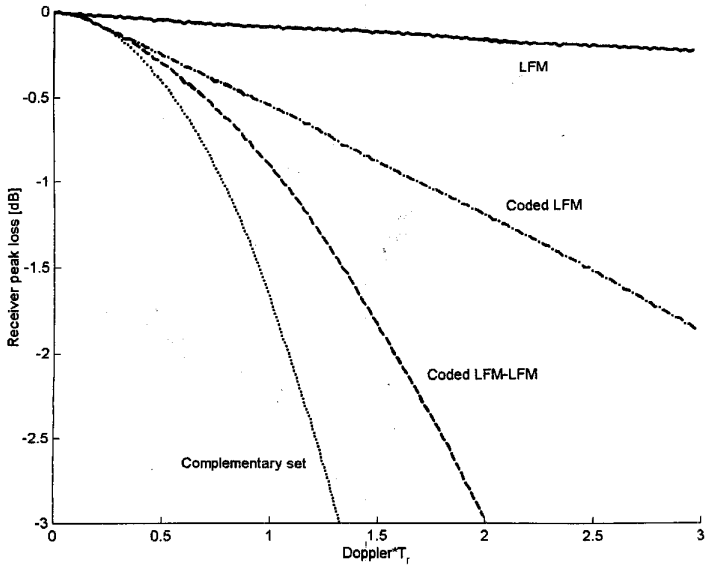

Fig. 26. Peak response FFT-based receiver loss for LFM pulse train, orthogonal coded LFM pulse train, orthogonal coded LFM-LFM pulse train, and train of complementary coded pulses for 128 points FFT used to minimize straddle loss (duty cycle is 1/3).

and taking out of the integral the parts that are not a function of t, gives

$$R(\tau)=\sum_{m=1}^{M}\sum_{k=1}^{M}\sum_{p=1}^{P}\sum_{q=1}^{P}a_{p,m}a_{q,k}^{*}\int_{0}^{PT_r}s_m[t-(p-1)T_r]\times s_k[t-\tau-(q-1)T_r]dt. \tag{8}$$

In order to get a simple expression for the ACF we assume $\tau\geq 0$ (the ACF is symmetric around zero delay) and define

$$\tau=rT_r+i_rt_s+\eta \tag{9}$$

where r is the integer part of T_r in τ ($r\geq 0$), i_r is the integer part of t_s in $\tau-rT_r$ ($0\leq i_r<T_r/t_s$), and η is the reminder of τ after division with t_s ($0\leq\eta<t_s$). We can write the ACF as

$$R(rT_r+i_rt_s+\eta)=\sum_{m=1}^{M}\sum_{k=1}^{M}\sum_{p=1}^{P}\sum_{q=1}^{P}a_{p,m}a_{q,k}^{*}\int_{0}^{PT_r}s_m[t-(p-1)T_r]\times s_k[t-\eta-i_rt_s-(q+r-1)T_r]dt. \tag{10}$$

Assuming $T_r>2T$ (duty cycle is below $\frac{1}{2}$) the multiplication of $s_m(t-(p-1)T_r)$ by $s_k(t-\eta-i_rt_s-(q+r-1)T_r)$ is zero for all m, k, t, η, i_r, and $p\neq q+r$. Thus we can write the ACF as

$$R(rT_r+i_rt_s+\eta)=\sum_{m=1}^{M}\sum_{k=1}^{M}\sum_{p=r+1}^{P}a_{p,m}a_{p-r,k}^{*}\int_{0}^{PT_r}s_m[t-(p-1)T_r]\times s_k[t-\eta-i_rt_s-(p-1)T_r]dt. \tag{11}$$

Changing the variable in the integral we can write

$$R(rT_r+i_rt_s+\eta)=\sum_{m=1}^{M}\sum_{k=1}^{M}\sum_{p=r+1}^{P}a_{p,m}a_{p-r,k}^{*}\int_{-(p-1)T_r}^{PT_r-(p-1)T_r}s_m(t)s_k(t-\eta-i_rt_s)dt. \tag{12}$$

For the integrand not to be zero we must have that $s_m(t)$ is not zero or that $0\leq(m-1)t_s\leq t<mt_s\leq Mt_s$. Since the integrals' lower limit is negative and the upper limit is at least $T_r>Mt_s$ for all p we can replace the integral lower limit with $(m-1)t_s$ and the upper limit with mt_s without changing the result.

The autocorrelation can thus be written as

$$R(rT_r+i_rt_s+\eta)=\sum_{m=1}^{M}\sum_{k=1}^{M}\sum_{p=r+1}^{P}a_{p,m}a_{p-r,k}^{*}\int_{(m-1)t_s}^{mt_s}s_m(t)s_k(t-\eta-i_rt_s)dt \tag{13}$$

where the integral is not a function of p or r. When summing over all possible values of m and k the integrand will not be zero only for $(k-1)t_s\leq t-\eta-i_rt_s<kt_s$. Using the limits of the integral we can also write that $mt_s>t\geq\eta+i_rt_s+(k-1)t_s>t-t_s\geq(m-2)t_s$. For a given delay ($i_r$ and η are fixed) and m we get that the integral will be non-zero only for at most two values of k that solve $m-\eta/t_s-i_r+1>k>m-i_r-\eta/t_s-1$. Denote these two values of k by $k_1=m-i_r-1$ and $k_2=m-i_r$. Note that in the case where $\eta=0$ we get only one value of $k=k_2=m-i_r$ and that k must also be between 1 and M.

We can solve the integral explicitly for $k=k_1=m-i_r-1$ (denote this by I_1) and $k=k_2=m-i_r$ (denoted I_2). For mathematical simplicity we also

define I_1 and I_2 to be zero when the value of k is not between 1 and M.

This gives I_1 and I_2 as

$$I_1 = \begin{cases} \int_{(m-1)t_s}^{(m-1)t_s+\eta} s_m(t)s_{m-i_r-1}(t-\eta-i_r t_s)dt & 1 \le m-i_r-1 \le M \\ 0 & \text{otherwise} \end{cases} \quad (14)$$

and

$$I_2 = \begin{cases} \int_{(m-1)t_s+\eta}^{mt_s} s_m(t)s_{m-i_r}(t-\eta-i_r t_s)dt & 1 \le m-i_r \le M \\ 0 & \text{otherwise} \end{cases}. \quad (15)$$

Note that when $\eta = 0$, $I_1 = 0$ which coincides with our previous observation on the case of integer τ/t_s. In this stage we write our first useful result.

Result 1. The ACF for any positive delay τ is given by

$$R(rT_r + i_r t_s + \eta) = \sum_{m=1}^{M}\left(I_1 \sum_{p=r+1}^{P} a_{p,m}a^*_{p-r,m-i_r-1} + I_2 \sum_{p=r+1}^{P} a_{p,m}a^*_{p-r,m-i_r}\right) \quad (16)$$

where I_1 and I_2 are were given in (14) and (15) and r, i_r and η were defined in (9).

PROOF Since I_1 and I_2 are not a function of p or r the result comes directly from (13) and the definition of I_1 and I_2.

Result 2. The partial ACF in the area of the mainlobe ($0 \le \tau \le T_r - T$) is given by

$$R(\tau) = \begin{cases} \sum_{m=1}^{M} \|a_m\|^2 R_m(\tau) & 0 \le \tau < t_s \\ 0 & t_s \le \tau < T_r - T \end{cases} \quad (17)$$

where $\|a_m\|^2$ is the square of the norm of the mth column in matrix $\mathbf{A}$ and $R_m(\tau)$ is the ACF of $s_m(t)$.

PROOF First note that orthogonality of the columns of $\mathbf{A}$ implies that

$$\sum_{p=1}^{P} a_{p,m}a^*_{p,k} = \delta(m-k)\sum_{p=1}^{P}|a_{p,m}|^2 = \delta(m-k)\|a_m\|^2 \quad (18)$$

where $\|a_m\|^2$ is the square of the norm of the mth column in matrix $\mathbf{A}$ and $\delta(x) = 1$ when $x = 0$ and zero otherwise.

Using the above and setting $r = 0$ in (16) gives

$$R(i_r t_s + \eta) = \sum_{m=1}^{M} \|a_m\|^2 [I_1\delta(i_r + 1) + I_2\delta(i_r)] \quad (19)$$

which implies that the autocorrelation for $r = 0$ is zero for all $i_r > 0$. Substituting I_2 gives the ACF for $0 \le \tau < t_s$ as

$$R(\eta) = \sum_{m=1}^{M} \|a_m\|^2 \int_{(m-1)t_s+\eta}^{mt_s} s_m(t)s^*_m(t-\eta)dt = \sum_{m=1}^{M} \|a_m\|^2 R_m(\eta) \quad (20)$$

and proves the result.

COROLLARY 1 *In the case of orthonormal phase coding matrix* $\mathbf{A}$ *the norm of any column in* $\mathbf{A}$ *is* P *and the partial autocorrelation can be written as*

$$R(\tau) = \begin{cases} P\sum_{m=1}^{M} R_m(\tau) & 0 \le \tau < t_s \\ 0 & t_s \le \tau < T_r - T \end{cases}. \quad (21)$$

Result 3. Adding a constant phase shift to any of the slices of the original pulse does not change the partial ACF in the area of the mainlobe ($0 \le \tau \le T_r - T$).

PROOF In order to prove the result it is sufficient to show that adding a constant phase to any of the slices does not change the ACF of the slice. Define $s_m(t) = \sigma_m(t)\exp(j\theta_m)$ where $\sigma_m(t)$ is any initial slice function and θ_m is the phase added to $\sigma_m(t)$. The ACF of $s_m(t)$ is given by

$$\begin{aligned} R_m(\tau) &= \int_{-\infty}^{\infty} s_m(t)s^*_m(t-\tau)dt \\ &= \int_{-\infty}^{\infty} \sigma_m(t)\exp(j\theta_m)\sigma^*_m(t-\tau)\exp(-j\theta_m)dt \\ &= \int_{-\infty}^{\infty} \sigma_m(t)\sigma^*_m(t-\tau)dt = \rho_m(\tau) \end{aligned} \quad (22)$$

where $\rho_m(\tau)$ is the autocorrelation of $\sigma_m(t)$.

Result 4. For an orthonormal phase-coded signal with identical slices, frequency modulating each slice with a frequency f_m results in a partial ACF that is given by

$$R(\tau) = \rho(\tau)\frac{1}{M}\sum_{m=1}^{M}\exp(j2\pi f_m\tau) \quad (23)$$

where $\rho(\tau)$ is the original orthonormal phase-coded pulse train partial autocorrelation for $0 \le \tau \le T_r - T$. Note that the result is multiplying the initial orthonormal phase-coded signal autocorrelation

with a windowing function that is a function of the modulating frequencies.

PROOF Define $s_m(t) = \sigma_m(t)\exp(j2\pi f_m t)$ where $\sigma_m(t)$ is any initial slice function and f_m is the modulating frequency of the mth slice. The ACF of $s_m(t)$ is given by

$$\begin{aligned} R_m(\tau) &= \int_{-\infty}^{\infty} s_m(t)s_m^*(t-\tau)dt \\ &= \int_{-\infty}^{\infty} \sigma_m(t)\exp(jf_m t)\sigma_m^*(t-\tau)\exp[-j2\pi f_m(t-\tau)]dt \\ &= \exp(j2\pi f_m\tau)\int_{-\infty}^{\infty} \sigma_m(t)\sigma_m^*(t-\tau)dt \\ &= \exp(j2\pi f_m\tau)\rho_m(\tau) \end{aligned} \tag{24}$$

where $\rho_m(\tau)$ is the autocorrelation of $\sigma_m(t)$. Using result 2 the partial ACF in the area of the mainlobe $(0 \le \tau \le t_s)$ is given by

$$R(\tau) = \sum_{m=1}^{M} \|a_m\|^2 R_m(\tau) = \sum_{m=1}^{M} \|a_m\|^2 \exp(j2\pi f_m\tau)\rho_m(\tau). \tag{25}$$

When orthonormal phase coding is used ($\|a_m\|^2 = P$) and when the original slices are identical ($\rho_m(\tau) = \rho_1(\tau)$) we get that

$$\begin{aligned} R(\tau) &= PM\rho_1(\tau)\frac{1}{M}\sum_{m=1}^{M}\exp(j2\pi f_m\tau) \\ &= \rho(\tau)\frac{1}{M}\sum_{m=1}^{M}\exp(j2\pi f_m\tau) \end{aligned} \tag{26}$$

which proves the result.

COROLLARY 2 *For an orthonormal phase-coded signal with identical slices, frequency modulating all slices with an identical frequency f results in a partial ACF that is given by*

$$R(\tau) = \rho(\tau)\frac{1}{M}\sum_{m=1}^{M}\exp(j2\pi f\tau) = \rho(\tau)\exp(j2\pi f\tau). \tag{27}$$

COROLLARY 3 *For an orthonormal phase-coded signal with identical slices, frequency modulating each slice with a linear function of the slice index ($f_m = m\Delta f$) results in a partial ACF that is given by*

$$\begin{aligned} R(\tau) &= \rho(\tau)\frac{1}{M}\sum_{m=1}^{M}\exp(j2\pi m\Delta f\tau) \\ &= \rho(\tau)\frac{\sin(\pi M\Delta f\tau)}{\sin(\pi\Delta f\tau)}\exp[j\pi\Delta f\tau(M+1)]. \end{aligned} \tag{28}$$

Note that when adding a constant frequency shift to all slices such that the average frequency shift is zero the exponent term vanishes. Note also that in order to reduce sidelobes the frequency deviation Δf should be selected such that the nulls of $\sin(\pi M\Delta f\tau)$ are close to the peaks of $\rho(\tau)$ outside the mainlobe.

COROLLARY 4 *For an orthonormal phase-coded signal with an even number of identical slices, frequency coding each slice such that half the slices get frequency modulation f and half the slices get frequency modulation $-f$ results in a partial ACF that is given by*

$$\begin{aligned} R(\tau) &= \rho(\tau)\frac{1}{M}\sum_{m=1}^{M}\exp(j2\pi f_m\tau) \\ &= \rho(\tau)\frac{1}{M}\left[\sum_{m\in M_0}\exp(j2\pi f\tau) + \sum_{m\notin M_0}\exp(-j2\pi f\tau)\right] \\ &= \rho(\tau)\cos(2\pi f\tau). \end{aligned} \tag{29}$$

Note that in a similar way using nonbinary frequency keying and different number of occurrence of each frequency can generate other shaping function.

REFERENCES

[1] Tseng, C. C., and Liu, C. L. (1972)
Complementary sets of sequences.
IEEE Transactions on Information Theory, **IT-18**, 5 (1972), 644–652.

[2] Frank, R. L. (1980)
Polyphase complementary codes.
IEEE Transactions on Information Theory, **IT-26**, 6 (1980), 641–647.

[3] Luke, H. D. (1985)
Sets of one and higher dimensional Welti codes and complementary codes.
IEEE Transactions on Aerospace and Electronic Systems, **AES-21**, 2 (1985), 170–179.

[4] Sivaswamy, R. (1978)
Multiphase complementary codes.
IEEE Transactions on Information Theory, **IT-24**, 5 (1978), 546–552.

[5] Sivaswamy, R. (1978)
Digital and analog sub-complementary sequences for pulse compression.
IEEE Transactions on Aerospace and Electronic Systems, **AES-14**, 2 (1978), 343–350.

[6] Kretschmer, F. F., Jr., and Gerlach, K. (1991)
Low sidelobe radar waveforms derived from orthogonal matrices.
IEEE Transactions on Aerospace and Electronic Systems, **27**, 1 (1991), 92–102.

[7] Popovic, B. M. (1990)
Complementary sets based on sequences with ideal periodic autocorrelation.
Electronic Letters, **26**, 18 (1990), 1428–1430.

[8] Golomb, S. W. (1992)
Two-valued sequences with perfect periodic autocorrelation.
IEEE Transactions on Aerospace and Electronic Systems, **28**, 2 (1992), 383–386.

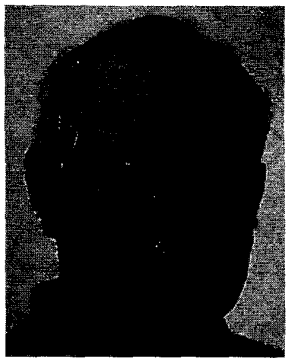

Nadav Levanon (S'67—M'70—SM'83—F'98) received a B.Sc. and M.Sc. degrees from the Technion–Israel Institute of Technology, in 1961 and 1965, and a Ph.D. from the University of Wisconsin–Madison, in 1969, all in electrical engineering.

He has been a faculty member at Tel Aviv University since 1970, where he is a professor in the Department of Electrical Engineering–Systems, and head of the Weinstein Research Institute for Signal Processing. He was chairman of the EE-Systems Department between 1983–1985. He spent sabbatical years at the University of Wisconsin, The Johns Hopkins University–Applied Physics Lab., and Qualcomm Inc., San Diego, CA.

Dr. Levanon is a member of the IEE, ION, and AGU. He is the author of the book *Radar Principles* (Wiley, 1988).

Eli Mozeson was born on May 26, 1970. He received his B.Sc. and M.Sc. degrees in electrical engineering from Tel-Aviv University, Israel, in 1992 and 1999, respectively. Since 1992 he serves in the Israeli Air Force as an electronic engineer. Currently, he is a Ph.D. student in the Department of Electrical Engineering–Systems, Tel-Aviv University. His area of interest is application of multicarrier phase-coded signals to radar systems.